

# Application of MPPT Controller with an Adaptive Neuro-Fuzzy Inference System for Fuel Cell Electric Vehicles

<sup>1</sup>Aradi Venkatesh

*Dept. of Electrical & Electronics Engineering,  
Anurag University,  
Venkatapur, Ghatkesar,  
Hyderabad, Telangana,  
India-500088.*

<sup>2</sup>D. Mohan Reddy

*Principal,  
Helapuri Institute of  
Technology & Science, Elur,  
West Godavari Dist, Andhra  
Pradesh, India-534450.*

<sup>3</sup>T Anil Kumar

*Dept. of Electrical & Electronics Engineering,  
Anurag University,  
Venkatapur, Ghatkesar,  
Hyderabad, Telangana,  
India-500088.*

**Abstract** – Because of stricter government guidelines aimed at reducing carbon emissions and improving fuel economy, the automotive industry is seeing an increase in the use of FCEVs. Proton exchange membrane fuel cells (PEMFC) may be controlled using an adaptive neuro-fuzzy inference system (ANFIS) that uses a high voltage-gain dc-dc boost converter to feed electric vehicles, according to this research. An adaptive neuro-fuzzy inference method is used to track the PEMFC's maximum power point in the proposed neural network MPPT controller (ANFIS). Converters with high switching frequencies and voltage gains are needed to power FCEV propulsion systems. A high voltage-gain interleaved boost converter is created here in order to attain high voltage gain. Reduces voltage and input current ripple on power semiconductor devices using this interleaving technology. The FCEV system's performance is compared to that of the MATLAB/Simulink platform's radial basis function network (RBFN) controller using an MPPT controller.

**Index Terms** - ANFIS, FCEV, Interleaving approach, MPPT, PEMFC.

## I. INTRODUCTION

Over the last decade, greenhouse-induced global warming has become increasingly worrisome. A major contributor to the greenhouse effect is thought to be an increase in carbon dioxide emissions, however this is no longer possible. Over 80% of worldwide energy consumption is accounted for by the use of fossil fuels, which are strongly linked to carbon emissions. The world's energy system must be modernised due to the finite nature of fossil resources. One of the most damaging pollutants to our environment is the greenhouse gas emissions from traditional fossil fuel-based automobiles as the number of vehicles on the road grows each year. Traditional internal combustion engines are growing their pollution outputs at an alarming rate [1–3].

There has been a growing belief that clean energy-based technology can help improve engine efficiency and reduce pollutant emissions as a whole. Fuel cell electric vehicles (FCEVs) use hydrogen as a new energy vector since it can be converted to electric energy and used as a new energy source to power them (FCEV). This technology has come a long way in the last ten years. FCEVs have higher upfront and continuing expenditures than EVs, HEVs, and PHEVs when compared to other types of electric vehicles (PHEV). In contrast, vehicles of this sort benefit from increased driving range, faster charging times, and virtually zero emissions. As a result, FCEVs are seen as a very promising and environmentally benign technology for promoting current modes of transportation [4]-[6]. A fuel cell's voltage and current characteristics are non-linear. In terms of output voltage and power, there is only one operating point for fuel cells that is optimal. The MPPT (maximum power point tracking) technique is the only way to maximise the output of a fuel cell. It is possible to discover the maximum power point by using particle swarm optimization, incremental conductance and fuzzy logic control (Sliding Mode Control, NN) and fuzzy logic tracking and control (MPP). MPPT's P&O algorithm is well-known for its simplicity and directness. [7]-[11] During steady-state operation, oscillations in the P&O and incremental conductance techniques lower the fuel cell system's efficiency.

An adaptive neuro-fuzzy inference system (ANFIS) and a radial basis function network controller (RBFN) are used to track the MPP. The MPPT controller of the PEMFC is proposed to be controlled by an ANFIS in this article (ANFIS). The front-end power conditioner of a fuel cell is sometimes referred to as a boost converter. To save on electricity, this is the instrument

of choice. High-power electronics can be employed with the standard boost converter. Thermal management issues and limited current handling may make a boost converter incompatible. To get around these problems, a number of DC-DC converters with significant voltage gains have been created. With minimum switching stress and high voltage gain, this work uses an interleaved boost converter (IBC). In addition to enhancing fuel cell reliability, interleaving technology significantly boosts the cell's power output [12- [15].

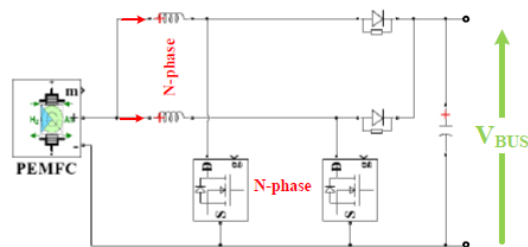
The structure of the paper is as follows. Boost converter interleaved setup is thoroughly examined in Section II. Section III focuses on the proposed system's modelling. Section IV focuses on simulation results and their discussion. Section V sums up the project's findings.

## II. CONFIGURATION OF WPT SYSTEM

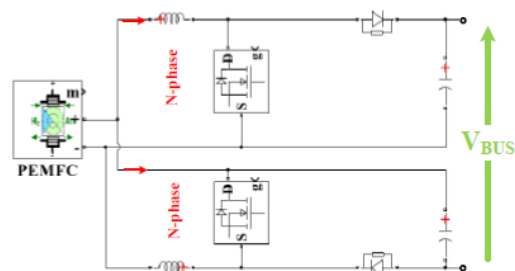
Researchers in the automotive industry are increasingly concentrating their efforts on developing vehicles that are both cost-effective and ecologically benign. Fuel cell electric cars and plug-in hybrid electric vehicles (PHEVs) are some of the most popular clean-energy vehicles now on the market (FCEVs). The market for electric, plug-in hybrid, and hybrid electric vehicles has increased dramatically from the early days of their development [16]-[18]. A rechargeable battery powers the electric motors that move EVs along, and they have several advantages over conventional internal combustion engines in terms of performance and cost. Both charging stations and electrical outlets can be used to charge PHEVs, which are hybrids. It is possible to classify both PHEVs and HEVs into two distinct categories: series PHEVs, or Parallel PHEV/HEVs, often known as hybrid vehicles, and extended range electric vehicles (EREVs). The electric motor is the only source of power that drives the wheels in series PHEVs/HEVs. The gasoline engine's sole by-product is electricity. Motors in PHEVs/HEVs are mechanically linked to the wheels and capable of either mechanical or electrical propulsion. [19],[20].

An internal combustion engine and an electric motor work together to produce significant fuel savings in HEVs. When coasting or braking, they use regenerative brakes to turn the energy that would otherwise be wasted into electricity. The IBC was designed to eliminate power source current ripple while maintaining the same voltage gain ratio as a conventional Boost converter, as seen in Fig. 1(a). Figure 1 shows one example of this. Multiple parallel power switch input currents are therefore shared. Overall conversion efficiency can be improved while stress on individual power switches is reduced as a result.

An IBC capable of producing 150kW in two-phase hybrid mode has been indicated by Wen et al. According to Benyahia et al., a 500W three-phase IBC prototype was investigated using an MPPT controller. When it came to optimising the motor voltage and fuel cell stack cell count, Toyota Maria went with a 4-phase IBC. To reduce power source current ripple and increase voltage gain ratio, the floating interleaved boost converter (FIBC), indicated in Figure 1b, has been widely explored for FCEV applications. The control layout, on the other hand, is more complicated than with the IBC. A novel 50kW prototype floating interleaved Buck-Boost Converter (FIB-BC) was recently reported by Gao et al. for fuel cell electric vehicle applications, as indicated in Fig 1. (c). Reducing current ripple and increasing efficiency and reliability by switching between step-up and step-down modes was made possible by a new topology. There was a 95 percent efficiency rate, which means that the process was highly efficient (Si-based IGBT).



(a) N-phase IBC



(b) N-phase FIBC

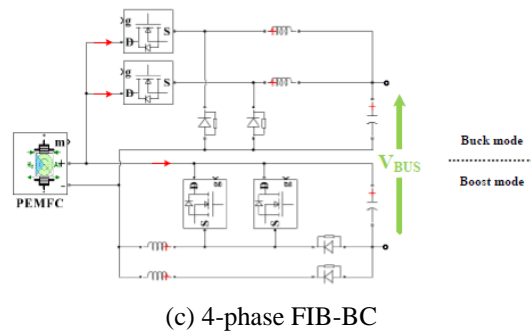


Fig. 1. DC/DC converter schematics based on interleaved architectures for non-isolated FCEV applications

### III. SYSTEM MODELING

Electric motors can be powered by an inverter fed by the converter's output voltage. The electric motor is critical in FCEVs. When the motor is adequate, the fuel cell's cost and size are greatly decreased. Most automakers traditionally used DC motors in electric car applications. DC motors are inefficient and expensive to maintain because of the numerous brushes and revolving parts. Due to the ease of control, great dependability, and longevity of permanent magnet BLDC motors, they are now the preferred choice for FCEV applications because of their wide range of applications. The three-phase high voltage gain IBC driven by a BLDC motor FCEV system indicated in Figure 2 is an interesting concept. PEMFC, three-phase high voltage gain IBC, VSI and BLDC motor make up the system. In order to link the PEMFC and VSI, an IBC with three phases is used. ANFIS-based MPPT optimises fuel cell output by taking this into account. An IBC three-phase VSI drives the BLDC motor. The VSI switches are controlled by a BLDC motor's electronic commutation. The vehicle's wheels are connected to the vehicle's motor shaft for propulsion.

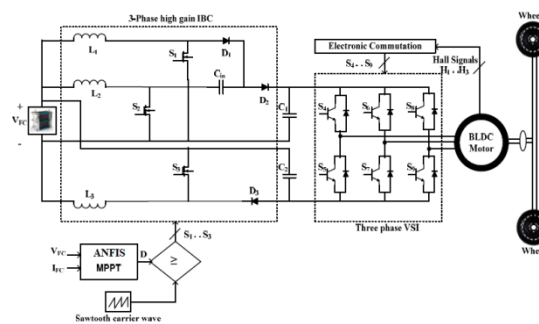


Fig. 2. Fuel cell powered electric car with BLDC motors, as proposed in this design.

#### A. Fuel cell modeling

Hydrogen fuel is used in fuel cells, an electrochemical device that generates electricity. As inputs, fuel cells use air and fuel, which are then chemically transformed into water and power by the reaction of these two substances. The fuel cell's architecture includes an electrolyte and two electrodes (anode and cathode). Hydrogen ions are separated into positive and negative charges by an electrolyte solution. When hydrogen and oxygen are delivered into the cell, electricity is generated at the cell's output.

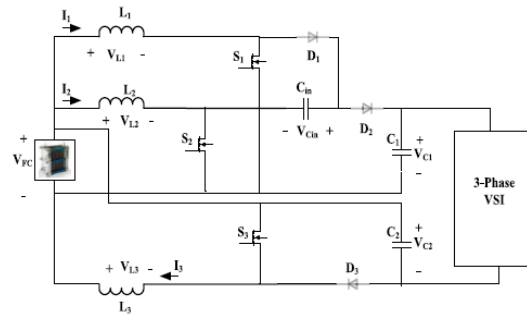
#### B. Three-phase high voltage gain IBC

S1, S2, and S3 comprise the three components of the converter (D1, D3 and D2). The letters L1, L2, and L3 are used to identify the inductors in each of the three phases of the filtering process. The input voltage is  $V_{FC}$ , the output voltage is  $V_O$ , and the load resistance is  $R$  in this circuit. Using these assumptions, the suggested high voltage gain is analysed. IBC:

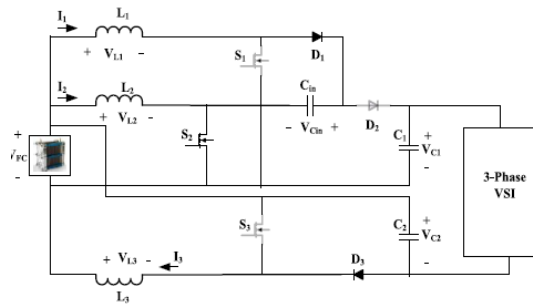
i) There should be no issues with any of the three phase inductors (L1 D L2 D L3 D L). It is also possible to use the two capacitors that are used in filtering interchangeably (C1 D C2 D C). iii) The converter under consideration can only operate in Continuous Conduction Mode (CCM). iv) We can assume that voltage and current ripples are insignificant because the capacitor and inductor are small in size. Two 180-phase shifted gate pulses engage switches S1, S2, and S3. While switches S1 and S2 receive a single gate pulse, switch S3 receives a gate pulse with a 180-degree phase shift for example, Fig. 3 shows the proposed converter's many operating modes.

Mode-1: According to Fig. 3, S1, S2, S3, and all three diodes are reverse biased, which means that all three switches have been turned on (a). Input voltage source VFC is the only source of voltage for all three inductors.  $(VFC/L)$  sloping currents of I1, I2, and I3 climbed linearly. The input capacitor Cin must be kept away from both the load and the power supply. When the load is removed, the load resistor charges the VC1 and VC2 output caps with energy and the voltages drop with the slope of  $(VO/RC)$ .

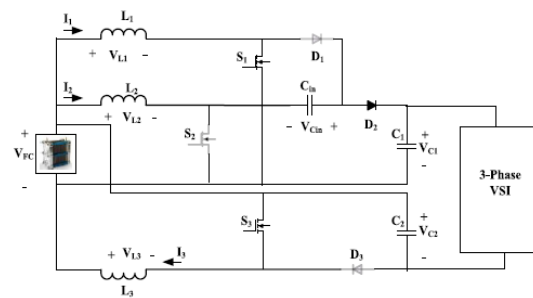
In this mode, none of the three switches (S1, S3, and S2) are activated. Diodes D1 and D3 are both biased forward, but diode D2 is biased backwards, as indicated in Fig. 3(b) (b). The current flowing through the inductors L1 and L3 was lowered by a slope of  $(VFC*VCin)/L$  and  $(VFC*VC2)/L$ . The current flowing through the inductor L2 increases as the slope of  $(VFC/L)$  increases. The voltage VFC supplied to C2 and Cin causes them to be charged.



(a)



(b)



(c)

Fig. 3. 3-phase high voltage gain IBC operation modes

Mode-3: Switch S2 is turned off in this mode. The switch S1 has a green light. D1 and D3 are biased in the opposite direction to D2, which is conducting, as seen in Fig. 3. (c). While L1 and L3 are being charged, their current increases with a slope of  $(VFC/L)$  due to an input voltage source VFC. When the current via the inductor L2 declines,  $VCin/L$  is the slope at which the current flows. The C2 and Cin capacitors receive load power. VFC supplies power to charge capacitor C1 via capacitor C1.

#### IV. SIMULATION RESULTS

In order to test the proposed FCEV system's performance when powered by a BLDC electric motor, the MATLAB/Simulink platform is used.

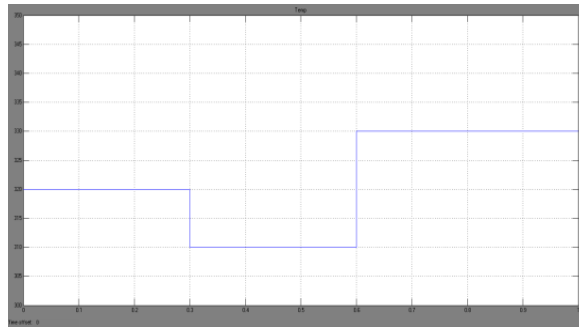
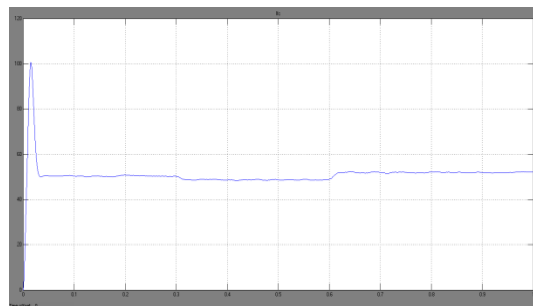
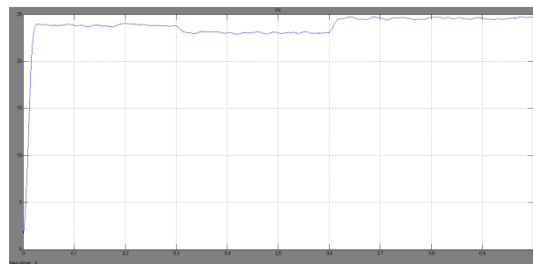


Fig. 4. Changes in the PEMFC system's temperature

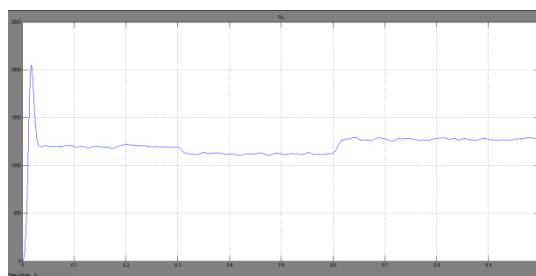
The abrupt fluctuations in fuel cell temperature are taken into account as follows in order to analyse the FCEV system's dynamic reaction.  $T = 320^{\circ}\text{K}$  for a period of 0 to 0.3sec,  $T = 310^{\circ}\text{K}$  for a period of 0.3 sec to 0.6 sec and  $T = 330^{\circ}\text{K}$  for a period of 0.6sec to 0.9 sec as indicated in Fig. 4.



(a).  $I_{FC}$  waveform



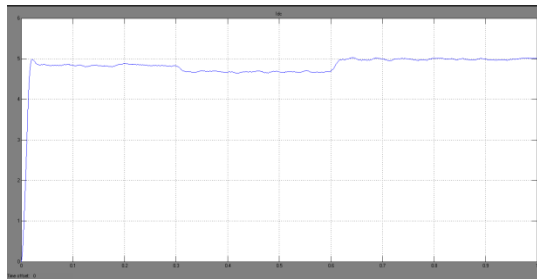
(b).  $V_{FC}$  waveform



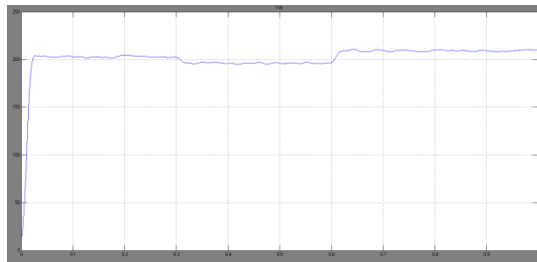
(c).  $P_{FC}$  waveform

Fig. 5: Fuel cell output current, voltage, and power at varying temperatures.

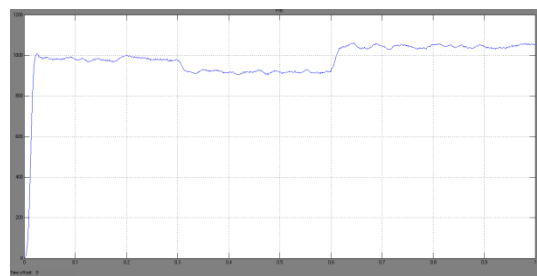
For varied temperatures, Fig5 shows the output current, voltage, and power waveforms of the fuel cell. The fuel cell can produce temperatures of 108<sup>0</sup>K for 0–0.3 seconds, 970W for 0.3–0.6 seconds, and 122<sup>0</sup>K for 0.6–0.9 seconds.



(a).  $I_{dc}$  waveform



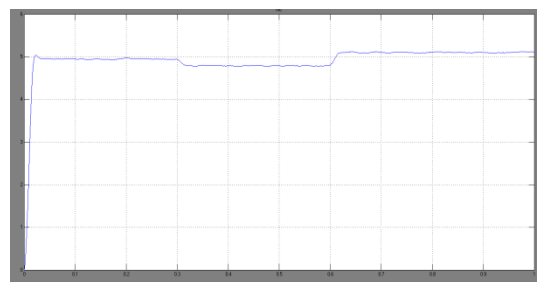
(b).  $V_{dc}$  waveform



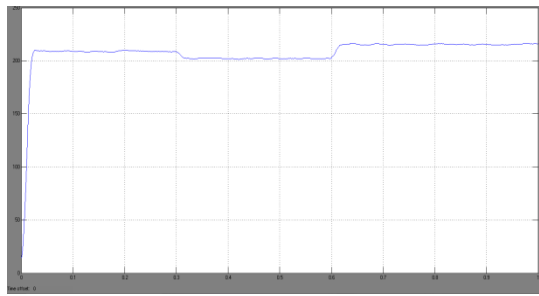
(c).  $P_{dc}$  waveform

Fig. 6. The DC link output current, voltage, and power at various temperatures utilising RBFN

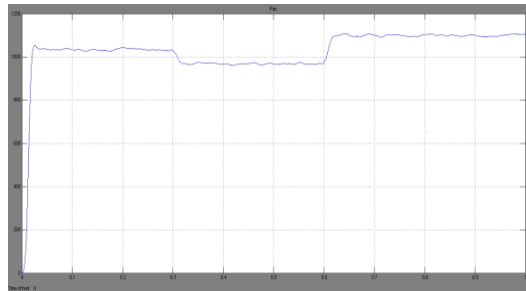
DC link current, voltage, and power are indicated in Fig. 6 by utilising the RBFN basis MPPT method. For temperatures of 320<sup>0</sup>K, 310<sup>0</sup>K, and 330<sup>0</sup>K, it generates a power of 1000W, 830W, and 1150W, correspondingly.



(a).  $I_{dc}$  waveform



(b).  $V_{dc}$  waveform



(c).  $P_{dc}$  waveform

Fig. 7. DC link o/p current, voltage & power at different temperatures using ANFIS

DC link output current, voltage, and power are all controlled by an ANFIS MPPT controller (Fig 7). 1050W is provided for 320<sup>0</sup>K, 900W for 310<sup>0</sup>K and 1200W for 330<sup>0</sup>K by the suggested controller.

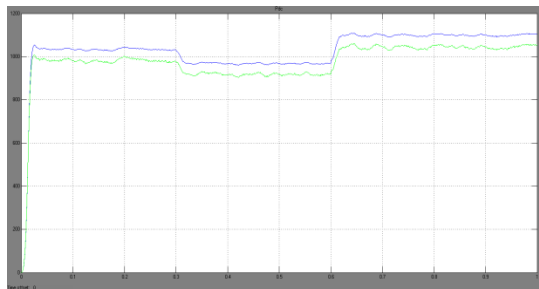
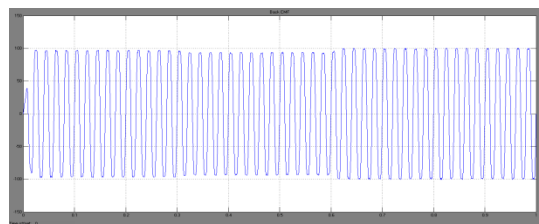
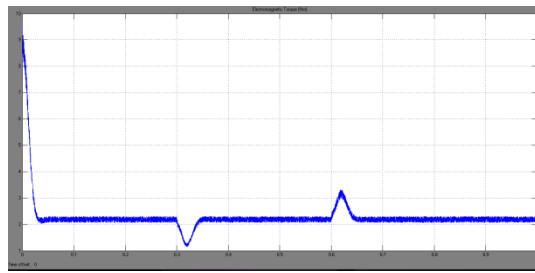


Fig. 8: Comparison of DC link power with both ANFIS and RBFN based MPPT controllers ( $P_{dc}$ )

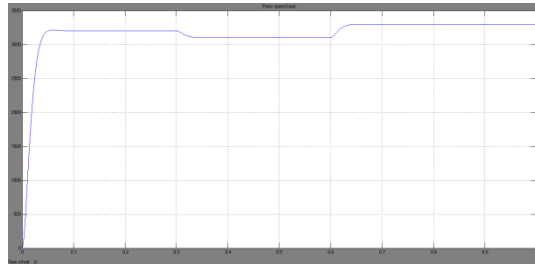
Figure 8 compares a fuel cell MPPT controller based on ANFIS with one based on RBFN. According to the predictions (see Figure 8), the suggested controller generates more DC link power than the RBFN.



(a). Back EMF (E)



(b). Electromagnetic Torque ( $T_e$ )



Speed (N)

Fig. 9. BLDC motor results

Figure 9 depicts the BLDC motor's properties at various fuel cell temperature ranges. Is<sub>a</sub> current, return EMF,  $T_e$  electromagnetic torque, and  $T_L$  load torque (TL) are all indicated when the fuel cell is operating at a temperature greater than ambient. Starting at 3300 RPM, the BLDC motor then spins at 2400 RPM for 0.9 seconds before returning to 3700 RPM. The torque of a BLDC motor is unaffected by variations in speed.

## V. CONCLUSION

This study proposes a three-phase high voltage gain DC-DC converter for use in FCEV applications. As a result of the proposed converter, input current ripples in fuel cells and voltage stress on power semiconductor switches were greatly reduced. MPPT for a 1.26 kW PEMFC is created using the ANFIS-based MPPT technique to maximise power extraction at varied temperatures. Comparing the RBFN MPPT controller with the MPPT technique that has been proposed. There was a significant time difference between the ANFIS-based MPPT and the RBFN controllers when tracking maximum power, as indicated by simulations. Fuel cell system temperatures are also taken into consideration while evaluating the BLDC motor's performance aspects such as speed, electromagnetic torque and back EMF.

## REFERENCES

- [1] H.J. Chiu et.al., "A bidirectional DC-DC converter for fuel cell electric vehicle driving system," *IEEE Trans. Power Electron*, vol. 21, no. 4, pp. 950-958, Jul. 2006.
- [2] B. Geng et.al., "Combined power management/design optimization for a fuel cell/battery plug-in hybrid electric vehicle using multi-objective particle swarm optimization," *Int. J. Atom. Technol*, vol. 15, no. 4, pp. 645-654, 2014.
- [3] H. Hemi et.al., "A real time fuzzy logic power management strategy for a fuel cell vehicle," *Energy Convers. Manag*, vol. 80, pp. 63-70, Apr. 2014.
- [4] N. Mebarki et.al., "PEM fuel cell/battery storage system supplying electric vehicle," *Int. J. Hydrogen Energy*, vol. 41, no. 45, pp. 20993-21005, 2016.
- [5] S. Abdi et.al., "A novel approach for robust maximum power point tracking of PEM fuel cell generator using sliding mode control approach," *Int. J. Electrochemical. Sci.*, vol. 7, pp. 4192-4209, May 2012.
- [6] T. Eswam et.al., "Comparison of photovoltaic array maximum power point tracking techniques," *IEEE Trans. Energy Convers.*, vol. 22, no. 2, pp. 439-449, Jun. 2007.
- [7] S. Saravanan et.al., "Maximum power point tracking algorithms for photovoltaic system A review," *Renewable Sustainable Energy Rev.*, vol. 57, pp. 192-204, May 2016.
- [8] J. P. Ram et.al., "Design and overview of maximum power point tracking techniques in wind and solar photovoltaic systems: A review," *Renewable Sustainable Energy Rev.*, vol. 73, pp. 1138-1159, Jun. 2017.

- [9] L. N. Khanh et.al., "Power-management strategies for a grid-connected PV-FC hybrid system," *IEEE Trans. Power Del.*, vol. 25, no. 3, pp. 1874-1882, Jul. 2010.
- [10] A. Giustiniani et.al., "Low-frequency current oscillations and maximum power point tracking in grid-connected fuel-cell-based systems," *IEEE Trans. Ind. Electron.*, vol. 57, no. 6, pp. 2042-2053, Jun. 2010.
- [11] Wang et.al., "A novel magnetic coupling mechanism for dynamic wireless charging system for electric vehicles", *IEEE Transactions on Vehicular Technologies*, 2018, 67, (1), pp. 124–133.
- [12] Fujita et.al., "A dynamic wireless power transfer system applicable to a stationary system", *IEEE Transactions on Ind. Appl.*, 2017, 53, (4), pp. 3748–3757.
- [13] Sampath et.al., " design guidelines for high efficiency of wireless power transfer (WPT)," In proceedings of *2016 IEEE Region 10 Conference (TENCON)*, pp. 726-729. IEEE, 2016.
- [14] Varghese et.al., "Effects of coil misalignment in a four-coil implantable wireless power transfer system," In proceedings of *2016 IEEE 7th Power India International Conference (PIICON)*, pp. 1-6. IEEE, 2016
- [15] A. K. RamRakhyani et.al., "Design and Optimization of Resonance-Based Efficient Wireless Power Delivery Systems for Biomedical Implants," *IEEE Transactions on Biomedical Circuits and Systems*, vol. 5, pp. 48-63, 2011.
- [16] J. Kim et.al., "Optimal design of a wireless power transfer system with multiple self-resonators for an LED TV," *IEEE Transactions on Consumer Electronics*, vol. 58, pp. 775-780, 2012.
- [17] Sampath et.al., "Coil design guidelines for high efficiency of wireless power transfer (WPT)." In proceedings of *2016 IEEE Region 10 Conference (TENCON)*, pp. 726-729. IEEE, 2016.
- [18] Zhang et.al., "A Study of Effective Coupling Coefficient and Its Application to Evaluate the WPT Pads," In proceedings of *2019 IEEE 3rd International Electrical and Energy Conference (CIEEC)*, pp. 1568-1572. IEEE, 2019.
- [19] Li, Jie et.al., "Transmitter coil design for multi-load wireless power transfer systems," In proceedings of *2020 IEEE Energy Conversion Congress and Exposition (ECCE)*, pp. 1032-1038, 2020.
- [20] G. Lazzi et.al., " "Thermal effects bio implants," *IEEE Engineering in Medicine and Biology Magazine.*, pp. 75–81, Sep. 2005.